High-performance plasmonic refractive index sensors via synergy between annealed nanoparticles and thin films

To cite this article before publication: Zhaowei Zhu *et al* 2020 *Nanotechnology* in press https://doi.org/10.1088/1361-6528/ab7531

High-performance plasmonic refractive index sensors via synergy between annealed nanoparticles and thin films

Zhaowei Zhu, Yusheng Ding, Zixi Wang, Chuantong Cheng*, Decai Li, Hongda Chen*

Dr. Zhaowei Zhu, Prof. Zixi Wang and Decai Li
State Key Laboratory of Tribology, Department of Mechanical Engineering, Tsinghua University, Beijing 100084, PR China
E-mail: zxwang@tsinghua.edu.cn
Dr. Chuantong Cheng, Prof. Hongda Chen
State Key Laboratory on Integrated Optoelectronics, Institute of Semiconductors, Chinese Academy of Sciences, Beijing, 100083, PR China
E-mail: chengchuantong@semi.ac.cn
Dr. Yusheng Ding
Aerospace Institute of Advanced Materials & Processing Technology, Beijing 100074, People's Republic of China

Keywords: refractive index sensors, particle-on-film structure, transfer process, low cost, high stability

Plasmonic nanostructure-based refractive index (RI) sensors are the core component of biosensor systems and play an increasingly important role in the diagnosis of human disease. However, the costs of traditional plasmonic RI sensors are not acceptable to everyone due to their expensive fabrication process. Here, a novel low-cost and high-performance visible-light RI sensor with a particle-on-film configuration was experimentally demonstrated. The sensor was fabricated by transferring annealed Au nanoparticles (NPs) onto a thin gold film with polymethyl methacrylate (PMMA) as a support. RI sensitivities of approximately 209 nm/RIU and 369 nm/RIU were achieved by reflection and transmission spectrum measurements, respectively. The high sensitivity is due to the strong plasmon-mediated energy confinement within the interface between the particles and the film. The possibility of wafer-scale production and high working stability achieved by the transfer process, together with the high sensitivity to the environmental RI, provides an extensive impact on the realization of universal biosensors for biological applications.

1. Introduction

The excitation of collective oscillations of the electronic charge density in metallic

structures results in surface plasmon resonances (SPRs), which are electromagnetic oscillations known as surface plasmon polaritons (SPPs) [1]. SPRs usually occurs in two types: propagating SPRs (PSPRs), which exist along the metal–dielectric interface and localized SPRs (LSPRs), which can be excited in metallic nanoparticles [1-3]. With extremely high sensitivity to the refractive index (RI) of the surrounding dielectric medium, PSPRs are fully utilized in most of the commercially available plasmon resonance-based biosensors [4-10]. However, the momentum match between photons and plasmons should be satisfied by using additional fabrication steps or optical devices for the excitation of SPPs, which leads to a complicated fabrication process and high cost [11,12]. In addition, owing to the relatively weaker local electric field, PSPR-based biosensors always have difficulty in achieving high sensitivity for the detection of small analytes [13,14]. In contrast to PSPRs, on the one hand, LSPRs in single metallic nanoparticle can be easily excited and bring about strong enhancement of the local electric field; on the other hand, LSPR-based sensors often show very high sensitivities to the concentration changes of small analytes due to the smaller penetration depth of the evanescent electric field [15-19]. However, LSPR-based sensors often show relatively low sensitivity to the RI of the surrounding dielectric medium because of their small electromagnetic fields decay length [20-21].

The plasmonic performance of particle-on-film configurations has received increasing attention, and many theoretical and experimental works have been performed to study the plasmonic effects in particle film geometries [22-31]. The direct excitation of SPPs by incident light is achieved with the help of nanoparticles, which means that the configurations can support PSPRs and LSPRs simultaneously. Moreover, the strong coupling of PSPRs and LSPRs results in a notable enhancement in the electric field and prominent sensitivity to the RI change [32-38]. However, except for a small number of applications in surface plasmon enhanced light scattering, these excellent properties have not been fully utilized until now [39-45]. The main obstacle to the mass production of highly sensitive plasmonic sensors is the

requirement of costly equipment and long times to define large areas of well-proportioned NPs on a metal film. To decrease the cost of the fabrication of NPs on metal films, some groups have tried to span commercial NPs on a metal film. However, the uniformity and stability of the spun NPs do not meet the consistency and repeatability requirements of a sensor. Another cost-effective method used to obtain uniformity NPs on metal films is called colloidal lithography and with this technology Antohe et al. proposed a high performance reflection-type fiber-optic sensors [46].

Annealed Au NPs with crystallization structure are good choice for optical sensing applications due to the high stability, low extinction loss and scalable fabrication [47-50]. Uniform Au NPs can be obtained easily by putting a quartz substrate with a nanometer-thick metal film into a high-temperature annealing furnace. With optimization annealing technology, annealed Au NPs-dielectric-Au film based sensors may be achieved. However, the Au film properties may be affected by the relative high annealing temperature. What's more, the working stablity of the sensor can not be guaranteed as the adhesion between annelaed Au NPs and dielectric layer is very weak. Hence, fixing annealed metal NPs on metal films with a low temperature procrss is a problem that urgently needs to be solved.

In this work, we fabricated particle-on-film configurations just by transferring large areas of annealed Au NPs onto Au films with the previous reported polymethyl methacrylate (PMMA)-assisted transfer process [51, 52]. And the the annealed Au NPs are successfully fixed on the Au film firmly with help of the PMMA material inside the gap between Au NPs and Au film. Hence, we report the first high-stablity visible-light RI sensor based on annealed Au particle-on-Au film configurations. Because of the high sensitivity of the plasmonic modes supported in the particle-on-film configurations to changes in the RI, ultrasensitive RI sensitivities of approximately 209 nm/RIU and 369 nm/RIU are obtained through the reflection and transmission spectrum measurements, respectively. Compared with annealed Au NPs, the particle-on-film configurations have achieved a more than approximately 2-fold

RI sensitivity enhancement. This transfer process makes the wafer-scale production of particle-on-film configurations a reality, which provides an extensive impact on the realization of low-cost and high-performance biological sensors due to the high sensitivity to the environmental RI and high working stability of the systems.

2. Materials and methods

The schematic fabrication process of visible-light RI sensors with a particle-on-film structure is shown in Fig. 1. Commercial quartzs (from Wuxi JingHe Optical Instrument CO., LTD.) with an area of 20×20 mm^2 are used as the substrate of the sensors, as shown in Fig. 1a. Actually, the size of the quartz substrate is unlimited, and large-scale production is achievable. The Si substrate is not suitable for the transfer of Au NPs as the interaction between Au NPs and Si substrate is very strong. Quartz with high transparency and low cost is very suitable material for optical sensor substrate. Hence, we chose quartz as the substrate in this work. Electron beam evaporation is utilized to obtain Au films with different thicknesses. The Au films on the surface of the 10 nm Ti adhesion layer shown in Fig. 1b have a thickness of 90 nm (for the reflection-type RI sensor) or 30 nm (for the transmission-type RI sensor) and function as the metal film in the particle-on-film configurations, while the Au film with a thickness of 14 nm shown in Fig. 1c is used to acquire the Au NPs in the particle-on-film configurations. The well-proportioned annealed Au NPs shown in Fig. 1d are obtained just by heating the 14 nm Au film at 600°C for 2 hours in an annealing furnace in an air atmosphere. A PMMA layer is then spun onto the annealed Au NP layer at a speed of 2000 r/min for 60 s, and then 180°C heating on a hotplate for 10 min is needed to fully wrap the Au NPs inside the PMMA support layer (Fig. 1e). A NaOH solution with a concentration of 2 mol/L is used to etch the quartz to obtain a free-standing PMMA/NP thin film, as shown in Fig. 1f. The PMMA/NP thin film is rinsed with deionized water several times to remove the oxide etch residues and then fished by a prefabricated Au film (Fig. 1 g). Another heating step at 180°C for 15 min is carried out to achieve full contact between the PMMA layer and the

Au film. Finally, ultrasonic cleaning in acetone, ethanol and deionized water with a power of 50% for 10 min each is used to remove all the PMMA on the surface of the Au particles and Au film (Fig. 1h). Excitingly, the PMMA layer between the Au NPs and Au film may not dissolved away completely, which will result in firm bonding between the Au particles and Au film and ultimately high working stability of the sensors. As the fabrication process can be achieved on a quartz substrate of arbitrary size, we can obtain large numbers of sensors in one procedure by a wafer saw, which shows the low cost of the sensors.

The testing system for the reflection and transmission spectra measurement is a self-built system based on Ocean Optics QE65000 spectrometer. The numerical aperture of the 50× OLYMPUS objective is 0.5. The simulation was performed with finite-difference time-domain (FDTD) solutions from Lumerical.

3. Results and discussion

Fig. 2a and 2b display the surface and cross-sectional scanning electron microscopy (SEM) images of the fabricated RI sensors, respectively. In order to show the Au NPs clearly, conductive silicon substrate was utilized to replace quartz substrate. The average diameter and height of the annealed Au NPs on the surface of the Au film are 100-200 nm and 40-70 nm, respectively. The SEM images of Au NPs before and afterthe PMMA-assisted transfer process is shown in Fig. S1(b) and (c). Compared with that of the original annealed Au NPs, the distribution of the transferred Au NPs did not change substantially, which means that this method can be used to transfer arbitrary nanostructures onto arbitrary substrates without any performance degradation of the nanostructures. The Au NPs are firmly fixed on the gold film with the assistance of the nanometer-thick PMMA layer at the interface. The SEM images and related EDS elemental distribution maps are displayed in Fig. S2. And C and O elementals can be discovered easily at the interface of Au NPs and Au film, which means the existence of the PMMA at the interface. To test the stability of the Au-based particle-on-film configurations, the chip was placed in an ultrasonic machine under 100% power for 30 min,

and no degradation was found. Fig. S1(c) and (d) show the SEM images before and after the sonication process. It is can be discovered form the images that almost no Au NPs were separated from the Au film during the sonication process. Hence, this kind of sensor can be reused for many times with easily sonication cleaning processes, resulting in low cost and a massive potential market.

Fig. 3a shows the measured normalized reflection spectra at normal incidence with air, water, ethanol and glycol on the surface of the particle-on-film configurations. The RI values of the medium materials we used here are 1, 1.333, 1.373, and 1.434, respectively. The position of minimum reflectivity is obviously changed as the RI of the system is changed. In addition, Fig. 3b shows the relationship between the minimum wavelength and the environmental RI. A linear relation can be observed, and an RI sensitivity of approximately 209 nm/RIU is achieved. The "error" bars were obtained with 9 measurements from 3 samples. Without the Au films, the peak position and the medium RI also obey a linear principle, and the RI sensitivity of the Au NPs is only approximately 100 nm/RIU [53, 54]. Hence, the introduction of the Au film leads to a more than 2-fold enhancement in the RI sensitivity of the Au NPs. To measure the RI sensitivity of the transmission spectra, the thickness of the Au film is decreased to 30 nm. Fig. 3c shows the measured normalized transmission spectra at normal incidence. Two peaks can be discovered: one peak at approximately 500 nm remains unchanged, and the other redshifts with increasing RI. And Fig. 3d shows the relationship between the changed peak wavelength and the environmental RI. A linear relation can be observed, and an RI sensitivity of approximately 369 nm/RIU is achieved. Hence, with the particle-on-film configurations, the RI sensitivity can be enhanced by approximately 300% for transmission spectra. In order to make a comparison in sensitivity for Au NPs on Au film configuration, uniform Au film configuration and Au NPs configuration, we have measured the reflection and transmission spectra at different RI for the 3 configurations. Figure S3 shows the reflection and transmission spectra at different RI for

14 nm Au film and annealed Au NPs. The RI sensitivity of annealed Au NPs is smaller than 100 nm/RIU, and the RI sensitivity of the 14 nm Au film is not obvious. Hence, particle on film configuration is suitable for high performance RI sensor. Au NPs often show a relatively low bulk RI sensitivity [55], however, a limit of detection of 0.01 ng/mL model antigen named bovine serum albumin under the optimized conditions has been achieved easily [56]. In our work, the RI sensitivity of Au NPs is enhanced by introducing the Au film. Hence, a better limit of detection than the former reported work will be achieved in the near future [56]. On the other hand, the resolution of spectrometer is about 10 pm, which means that the bulk RI resolution of our transmission-type RI sensor is estimated to be 2.71×10^{-5} RIU.

The high performance of the RI sensor results from the electromagnetic modes supported in the small gap between the Au NPs and the Au film. Fig. 4a shows the cross-sectional SEM, and gaps with heights of approximately 5 nm were clearly observed. The PMMA space layer in the gap works as a connection layer. Fig. 4b displays the electromagnetic mode in our designed structure (5 nm gap filled with PMMA material). The ultrahigh mode field intensity (more than 10-fold enhancement) in the gap can be easily observed, resulting in enhanced RI sensitivity of the particle-on-film configurations. We have also performed control simulations of the mode distribution of the plasmons for two structures: Au NP/5 nm air gap/Au film and Au NP/Au film (no gap). And the simulation results indicate that the mode field intensity of Au NP/5 nm air gap/Au film structure is much higher (43.2 vs 5.66, about 8 times) than that of Au NP/Au film structure (Fig. S4 (a) and (c)). Hence, air gap is better than PMMA gap, and PMMA gap is better than no gap. During the fabrication process, the PMMA located at the center of the NPs/film interface is probably remained (Figure S2), and much of the interface region may be air. Therefore, the mode field intensity of our fabricated sensor may be higher than the simulated results shown in Fig. 4b. In order to show the relationship between RI sensitivity and mode field intensity, a brief simulation of the reflectance spectrum as a function of the bulk refractive index of the surrounding medium has been performed (Fig.

S4 (b) and (d)). The simulation results tell that higher mode field intensity means higher RI sensitivity. In the simulation, the periodic boundary condition is utilized. The filed intensity in Fig. S4 (a) is obtained at wavelength of 605 nm and the Fig. S4 (c) is obtained at wavelength of 641 nm. As the size and distribution of the annealed Au NPs obtained in this work are not quite uniform, the simulation results are not completely consistent with the experiment results in quantitative analysis. Hence, further improvements are still possible while using the PMMA-assisted transfer process, with additional investigations in the achievement of more uniform annealed Au NP arrays and more suitable gap values [46, 57].

Finally, we discuss the importance of the novel plasmonic RI sensors proposed in this work and the potential advantages of introducing the transfer process into the fabrication of plasmonic nanostructure-based sensor devices.

(1) Low-cost and high-stability plasmonic RI sensor

Plasmonic sensors have been used in many commercial biosensor systems due to their small sample sizes and ability to achieve real-time dynamic monitoring [58, 59]. However, there is a positive correlation between the cost and stability of commercial plasmonic sensors. An RI sensor with high stability means a high cost, and the advantages of plasmonic sensors are not fully demonstrated. Developing a low-cost and high-stability plasmonic RI sensor is energetically great and imperative. This work prepared a novel RI sensor with a particle-on-film structure and a low-cost fabrication process and successfully achieved high device stability. Hence, the proposed RI sensor will find a large market in biosensor applications in the near future.

(2) Novel plasmonic nanostructure-based sensors

Different plasmonic nanostructures can support different plasmon modes and may show different sensing performances. Integrating different plasmonic nanostructures together may display new plasmon modes and enhanced sensing functions. In this work, we integrated Au NPs and Au films with a novel PMMA-assisted transfer process and obtained high-

performance and low-cost plasmonic RI sensors. Actually, with the proposed transfer process, arbitrary plasmonic nanostructures can be arranged together for enhanced sensing performance. Additionally, the gap between two different nanostructures can be as small as approximately 5 nm.

4. Conclusion

In conclusion, we developed a novel and cost-effective method for the fabrication of high-performance RI sensors with a Au NP-on-film structure. RI sensitivities of 209 nm/RIU and 369 nm/RIU were achieved by reflection and transmission spectrum measurements, respectively. This work not only proposes a successful strategy to obtain a low-cost metal NP-on-film structure for RI sensors but also establishes promising prospects in the domain of plasmonics-based SERS and biosensor applications.

Acknowledgements

Zhaowei Zhu and Yusheng Ding contributed equally to this work. The authors are grateful for the financial support from the National Key Research and Development Program of China (Grant Nos. 2018YFA0209000), the National Natural Science Foundation of China (Grant Nos. 61904173, 51735006), Aeronautical Science Fund of China (No. 20164058002), and Tsinghua University Initiative Scientific Research Program.

References

[1] Maier SA. Plasmonics: fundamentals and applications. Springer Science and Business Media, 2007.

[2] Surbhi L, Stephan L and Naomi J H 2007 Nano-optics from sensing to waveguiding Nat. Photonics 1 641-48

[3] Wu C, Alexander B K, Ronen A, Nihal A, Ahmet A Y, Hatice A and Gennady S 2011 Fano-resonant asymmetric metamaterials for ultrasensitive spectroscopy and identification of molecular monolayers Nat. Mater. 11, 69-75

[4] Shalabney A and Abdulhalim I 2012 Figure-of-merit enhancement of surface plasmon resonance sensors in the spectral interrogation Opt. Lett. 37 1175-77

[5] Srijit N, Carlos E and Ribal G S 2017 Crossed surface relief gratings as nanoplasmonic biosensors ACS Sens. 2 379-85

[6] Baiad M D and Kashyap R 2015 Concatenation of surface plasmon resonance sensors in a single optical fiber using tilted fiber Bragg gratings Opt. Lett. 40, 115-18

[7] Renoirt J M, Debliquy M, Albert J, Ianoul A and Caucheteur C 2014 Surface plasmon resonances in oriented silver nanowire coatings on optical fibers J. Phys. Chem. C 118 11035-42

[8] Law W, Yong K, Baev A and Prasad P N 2011 Sensitivity improved surface plasmon resonance biosensor for cancer biomarker detection based on plasmonic enhancement ACS Nano 5 4858-64

[9] Kim J A, Hwang T, Dugasani S R, Amin R, Kulkarni A, Park S H and Kim T 2013 Graphene based fiber optic surface plasmon resonance for bio-chemical sensor applications Sens. Actuators B Chem. 187 426-33

[10] Liu Z, Wei Y, Zhang Y, Wang Y, Zhao E, Zhang Y, Yang J, Liu C and Yuan L 2016 A multi-channel fiber SPR sensor based on TDM technology Sens Actuators B , 226 326-331

[11] Svedendahl M, Chen S, Dmitriev A and Kall M 2009 Refractometric sensing using propagating versus localized surface plasmons: a direct comparison Nano Lett. 9 4428-33

[12] Bolduc O R, Live L S and Masson J F 2009 High-resolution surface plasmon resonance sensors based on a dove prism Talanta 77 1680-87

[13] Prasad, P. N. Introduction to Biophotonics (Wiley-Interscience, 2003).

[14] Kabashin A V, Evans P, Pastkovsky S, Hendren W, Wurtz G A, Atkinson R, Pollard R, Podolskiy V A and Zayats A V 2009 Plasmonic nanorod metamaterials for biosensing Nat. Mater. 8 867-71

[15] Khan A U, Zhao S and Liu G 2016 Key parameter controlling the sensitivity of plasmonic metal nanoparticles: aspect ratio Phys. Chem. C 120 19353-64

[16] Gartia M R, Hsiao A, Pokhriyal A, Seo S, Kulsharova G, Cunningham B T, Bond T C and Liu G L 2013 Colorimetric plasmon resonance imaging using nano lycurgus cup arrays Adv. Opt. Mater. 1 68-76

[17] Chang T W, Wang X, Hsiao A, Xu Z, Lin G, Gartia M R, Liu X and Liu G L 2015 Bifunctional nano lycurgus cup array plasmonic sensor for colorimetric sensing and surface-enhanced raman spectroscopy Adv. Opt. Mater. 3 1397-404

[18] Li Q, Zhuo X, Li S, Ruan Q, Xu Q H and Wang J 2015 Production of monodisperse gold nanobipyramids with number percentages approaching 100% and evaluation of their plasmonic properties Adv. Opt. Mater. 3 801-12

[19] Kristof L, Willem V R, Gustaaf B, Liesbet L and Pol V D 2012 Boosting the figure-of-merit of lspr-based refractive index sensing by phase-sensitive measurements Nano Lett. 12 1655-59

[20] Jeffrey N A, Paige H, Olga L, Nilam C S, Zhao J and Richard P D 2008 Biosensing with plasmonic nanosensors Nature Mater. 7 442-53

[21] Amanda J H and Richard P D 2004 A unified view of propagating and localized surface plasmon resonance biosensors. Anal. Bioanal. Chem. 379 920-30

[22] Nordlander P and Prodan E 2004 Plasmon hybridization in nanoparticles near metallic surfaces Nano Lett 4 2209-13

[23] Papanikolaou N 2007 Optical properties of metallic nanoparticle arrays on a thin metallic film Phys. Rev. B 75 235426

[24] Garíca A F J 2007 Colloquium: light scattering byparticle and hole arrays Rev. Mod. Phys. 79 1267-90

[25] Kristy C V, Alison M F, Carolina N, Daniel E G, Paul M and Timothy J D 2010 Influence of particle-substrate interaction on localized plasmon resonances Nano Lett. 10 2080-86

[26] Stuart H R and Hall D G 1998 Enhanced dipole-dipole interaction between elementary radiators near a surface Phys. Rev. Lett. 80 5663-66

[27] Félidj N, Aubard J, Lévi G, Krenn J R,Schider G, Leitner A and Aussenegg F R 2002 Enhanced substrate-induced coupling in two-dimensional gold nanoparticle arrays Phys. Rev. B 66 245407

[28] Le F, Lwin N Z, Steele J M, KällN M and HalasP J 2005 Nordlander plasmons in the metallic nanoparticlefilm system as a tunable impurity problem Nano Lett. 5 2009-13

[29] He L, Smith E A, Natan M J and Keating C D 2004 The Distance-dependence of colloidal au-amplified surface plasmon resonance J. Phys. Chem. B 108 10973-80

[30] Mock J J, Hill R T, Degiron A, Zauscher S, Chilkoti A and Smith D R 2008 Distance-dependent plasmon resonant coupling between a gold nanoparticle and gold film Nano Lett. 2245-52

[31] Yamamoto N, Ohtani S and Garíca de A 2011 Gap and mie plasmons in individual silver nanospheres near a silver surface Nano Lett. 11 91-95

[32] Kristof L, Jef R, Willem V R, Gustaaf B, Liesbet L and Pol V D 2013 Tuning the fano resonance between localized and propagating surface plasmon resonances for refractive index sensing applications Plasmonics 8 1379-85

[33] Chen S, Meng L, Hu J and Yang Z 2015 Fano interference between higher localized and propagating surface plasmon modes in nanovoid arrays Plasmonics 10 71-76

[34] Mitradeep S, Mondher B, Julien M, Jean F B, Aurore O, Grégory B, Anne L C, Bernard B and Michael C 2015 Hybrid plasmonic mode by resonant coupling of localized plasmons to propagating plasmons in a kretschmann configuration ACS Photonics 2 237-45

[35] Christ A, Zentgraf T, Tikhodeev S, Gippius N, Kuhl J and Giessen H 2006 Controlling the interaction between localized and delocalized surface plasmon modes: experiment and numerical calculations Phys. Rev. B 74 155435

[36] Chang Y and Jiang Y 2014 Highly sensitive plasmonic sensor based on fano resonance from silver nanoparticle heterodimer array on a thin silver film Plasmonics 9 499-505

[37] Sachin K. S, Li A R, Li S Z and OrcidIbrahim A 2016 Optimal interparticle gap for ultrahigh field enhancement by LSP excitation via ESPs and confirmation using SERS J. Phys. Chem. C 120 28735-42

[38] Li A R, Sivan I, Ibrahim A and Li S Z 2015 Ultrahigh enhancement of electromagnetic fields by exciting localized with extended surface plasmons J. Phys. Chem. C 119 19382-89

[39] Chih T Y, Wu L, Liu X H, Nhung T T, Bai P, Bo L, Wang Y and Benjamin T 2016 Exploiting surface-plasmon-enhanced light scattering for the design of ultrasensitive biosensing modality Anal. Chem. 2016 88 11924-30

[40] Chih T Y, Wu L, Bai P and Benjamin T 2016 Investigation of plasmonic signal enhancement based on long range surface plasmon resonance with gold nanoparticle tags J. Mater. Chem. C 4 9897

[41] Chih T Y, Mohammad P M, Wu L, Bai P and Benjamin T Ultrasensitive detection of cancer prognostic mirna biomarkers based on surface plasmon enhanced light scattering 2017 ACS Sens. 2 635-40

[42] Min J K, Jaeyoung L, Alastair W W, Lee H J 2012 Nanoparticle-enhanced surface plasmon resonance detection of proteins at attomolar concentrations: comparing different nanoparticle shapes and sizes Anal. Chem. 84 1702-07

[43] Tomáš Š, Maria L E, Barbora Š, Jani J and Jiří H 2014 Enhancing sensitivity of surface plasmon resonance biosensors by functionalized gold nanoparticles: size matters Anal. Chem. 86 10350-56

[44] Law W, Yong K, Baev A and Prasad P N 2011 Sensitivity improved surface plasmon resonance biosensor for cancer biomarker detection based on plasmonic enhancement ACS Nano 5 4858-64

[45] Md Z H and Chris M M 2018 Gold nanoparticle-enhanced multiplexed imaging surface plasmon resonance (iSPR) detection of Fusarium mycotoxins in wheat Biosens. Bioelectron. 101 245-52

[46] Antohe (Arghir) I, Spasic D, Delport F, Li J Q and Lammertyn J 2017 Nanoscale patterning of gold-coated optical fibers for improved plasmonic sensing Nanotechnology 28 215301.

[47] Antohe (Arghir) I, Schouteden K, Goos P, Delport F, Spasic D and Lammertyn J 2016 Thermal annealing of gold coated fiber optic surfaces for improved plasmonic biosensing Sensors Actuators B 229 678–85.

[48] Ritu V, Rahul S, Jyotsna B, Heena I, Kumar Y, Amit K S, Plaisie J R, Gigli L and Ganesh D S 2019 Thermally induced plasmonic resonance of Cu nanoparticles in fullerene C70 matrix Vacuum 159 423-29

[49] Barman B, Dhasmana H, Verma A, Kumar A, Singh D N and Jain V K 2018 Substrates dependent low temperature fabrication of silver nanoparticles using rapid thermal annealing for light trapping application J. Nanosci. Nanotech. 18 7739-48

[50] Poonam S, Amit J, Avinashi K and Vinay G 2016 Thickness and annealing effects on the particle size of PLD grown ag nanofilms Plasmonics 11 669-75

[51] Liu Y, Cheng R, Liao L, Zhou H L, Bai J W, Liu G, Liu L X, Huang Y, Duan X F 2011 Plasmon resonance enhanced multicolour photodetection by graphene Nat. Commun. 2 579.

[52] Choi M, Kang G, Shin D, Barange N, Lee C W, Ko D H, and Kim K 2016 Lithography-Free Broadband Ultrathin Film Absorbers with Gap Plasmon Resonance for Organic Photovoltaics ACS Appl. Mater. Interfaces 8, 12997-13008.

[53] Chen H, Kou X, Yang Z, Ni W and Wang J 2008 shape- and size-dependent refractive index sensitivity of gold nanoparticles Langmuir 24 5233-37

[54] Mahmoud A M, Maysamreza C, Ali A and Mostafa A E 2012 Effect of the dielectric constant of the surrounding medium and the substrate on the surface plasmon resonance spectrum and sensitivity factors of highly symmetric systems: silver nanocubes J. Am. Chem. Soc 134 6434-42.

[55] Navas M P, Soni R K 2015 Laser-Generated Bimetallic Ag-Au and Ag-Cu Core-Shell Nanoparticles for Refractive Index Sensing *Plasmonics* 10 681–690.

[56] Jia K *et al* 2014 Strong Improvements of Localized Surface Plasmon Resonance Sensitivity by Using Au/Ag Bimetallic Nanostructures Modified with Polydopamine Films *ACS Appl. Mater. Interfaces* 6 219−227.

[57] Svedendah M, Verre R, Ka M 2014 Refractometric biosensing based on optical phase flips in sparse and short-range-ordered nanoplasmonic layers *Light: Sci. Appl.* 3 e220

[58] Pallarola D, Schneckenburger M, Spatz J P and Pacholski C 2013 Real-time monitoring of electrochemical controlled proteinadsorption by a plasmonic nanowire based sensor Chem. Commun. 49 8326

[59] Coskun A F, Cetin A E, Galarreta B C, Alvarez D A, Altug H and Ozcan A 2014 Lensfree optofluidic plasmonic sensor for real-time and label-free monitoring of molecular binding events over a wide field-of-view Sci. Rep. 4 6789

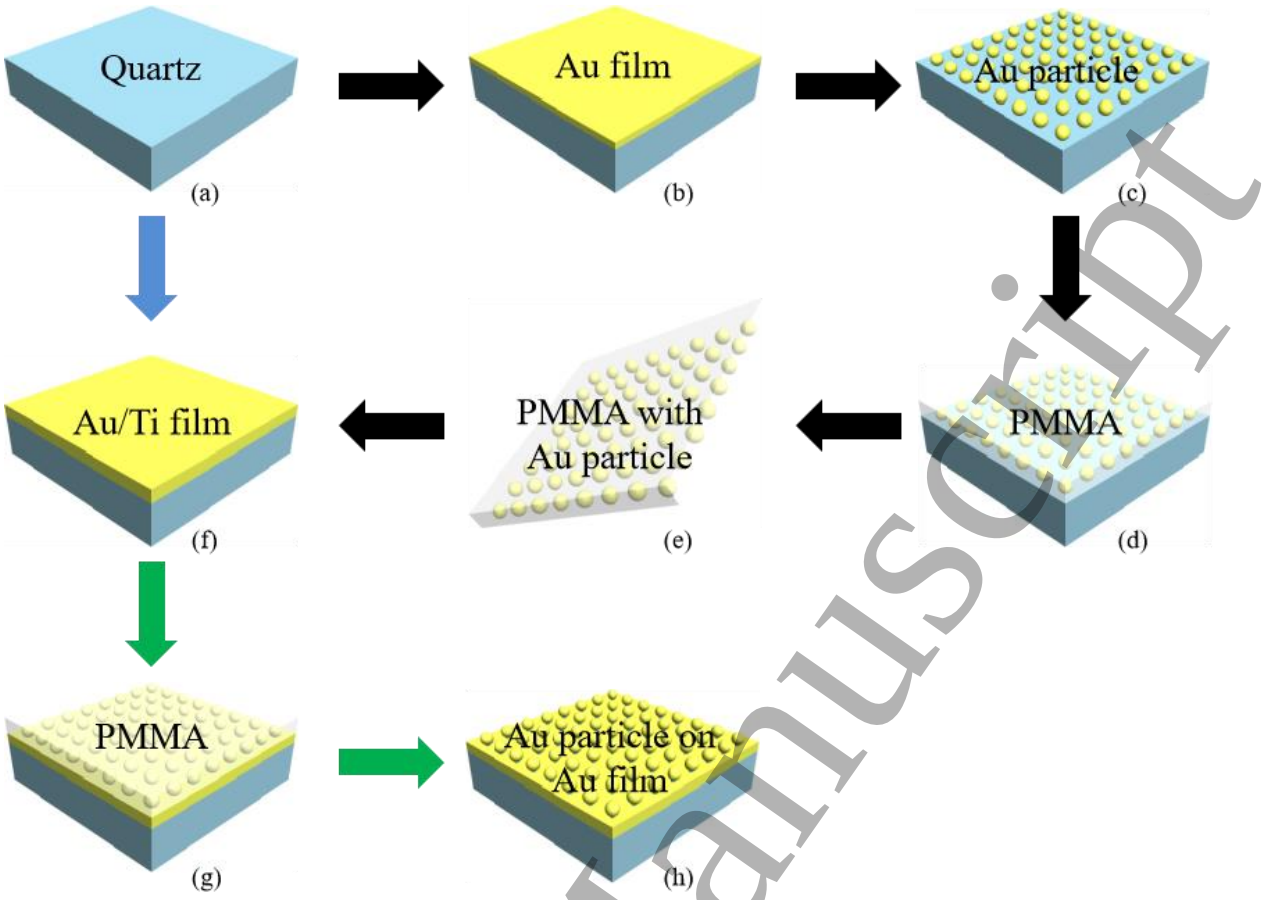

Figure 1. The schematic fabrication process of RI sensors with a particle-on-film structure. (a) Quartz substrate for RI sensors. (b) Au film prepared on the substrate. (c) Annealed Au NPs obtained on the substrate. (d) PMMA layer spun on Au NPs. (e) Au NPs supported by PMMA layer. (f) Au film prepared on the substrate. (g) PMMA layer transferred on Au film. (h) PMMA removed in acetone.

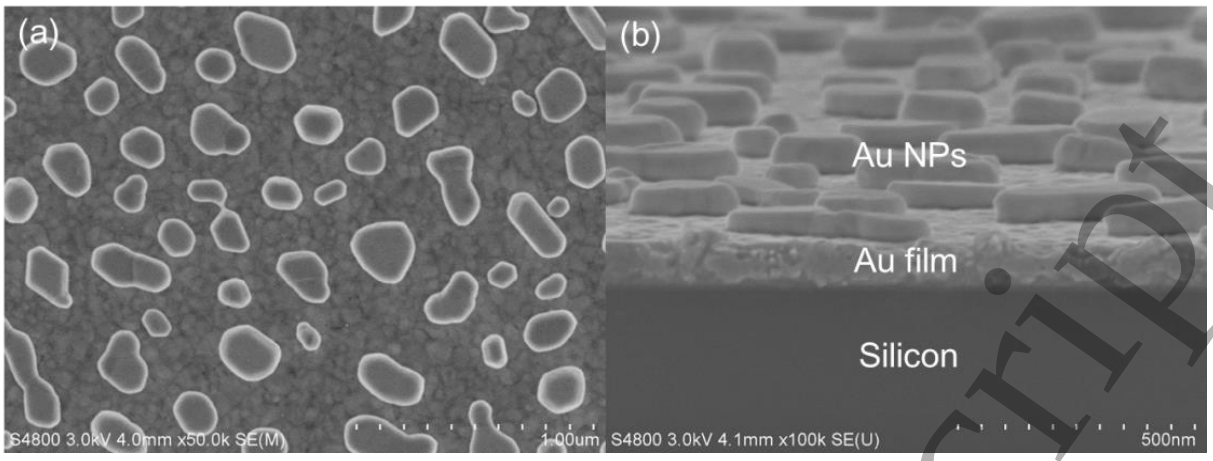

Figure 2. SEM images of the surface (a) and cross-section (b) of the fabricated structure with transfer process.

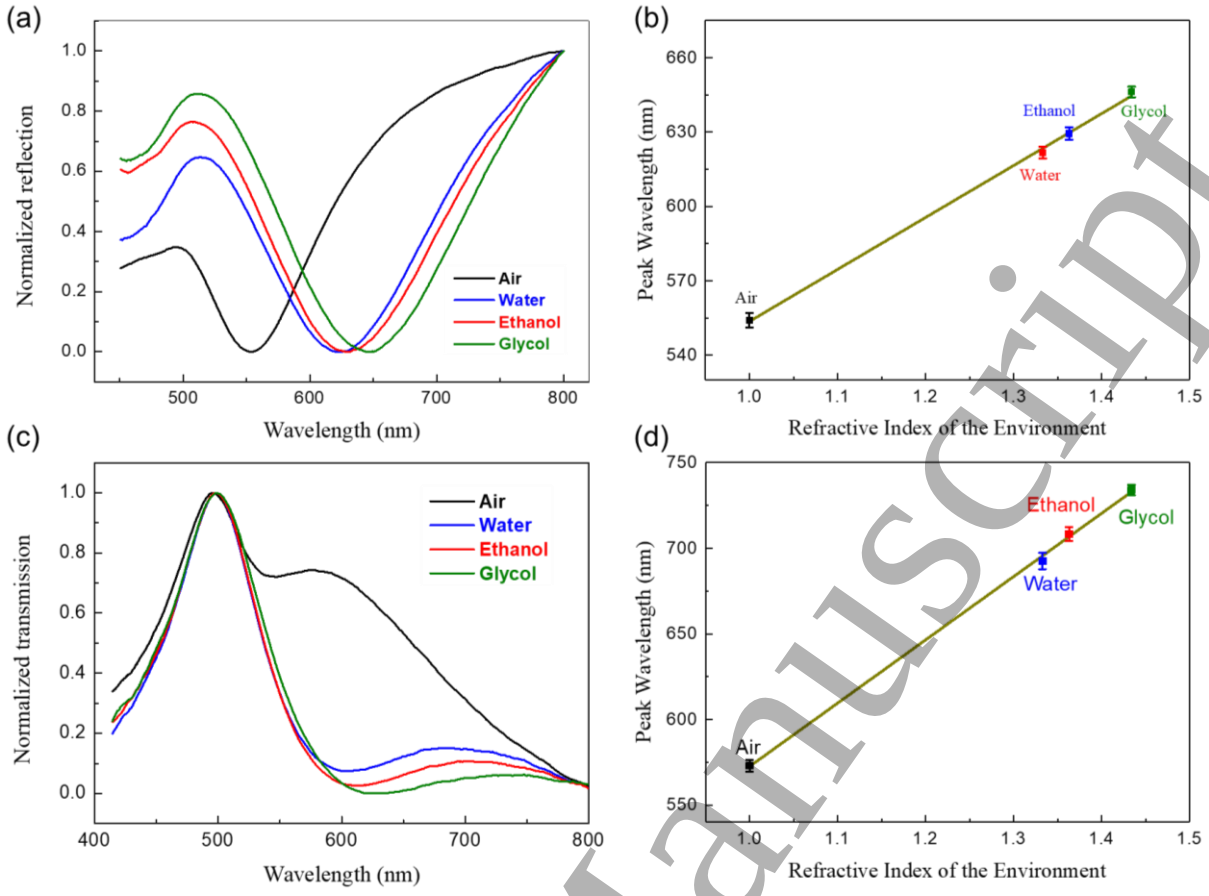

Figure 3. The measured reflection (a) and transmission (c) spectra for the Au particle-on-film configuration under different medium materials (air, water, ethanol, glycol). (b) and (d) show the relationship between peak wavelength and refractive of the environment in the reflection type and transmission type RI sensors, respectively.

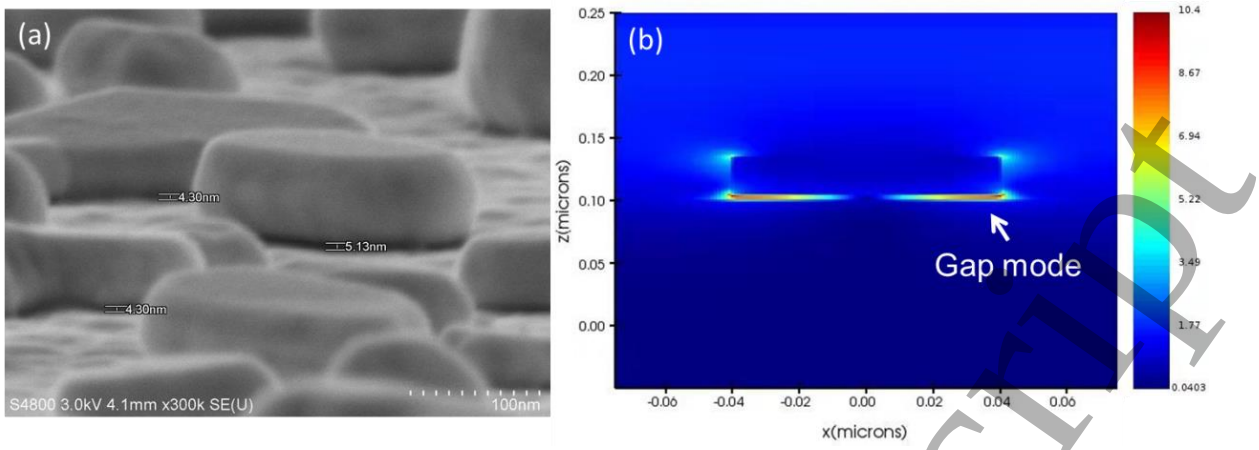

Figure 4. Cross-sectional SEM (a) and simulated plasmon gap mode (b) in the fabricated RI. sensors.